



An analysis of O–H interaction potentials, O–H and O–D collision cross sections, and vibrational states

Bernie D. Shizgal¹

Solar Terrestrial Environment Laboratory, University of Nagoya, Toyokawa, Aichi 442, Japan

Received 8 January 1998; received in revised form 25 May 1998; accepted 11 June 1998

Abstract

A detailed comparison of recently published OH, X²Π, ²Σ⁻, ⁴Π and ⁴Σ⁻ potentials is carried out. These potential functions are important in the accurate determination of O–H and O–D collision cross sections. The isotope effect in the O–H and O–D cross sections plays an important role in the enhanced nonthermal escape of H and D from Mars and Venus. The quantum mechanical elastic scattering cross sections for O–H and O–D collisions are determined with a set of potentials which are constructed with a new interpolation of the short range tabulated potentials and the long range asymptotic behaviour. The important role of the asymptotic radial variation of the potential functions in the determination of the elastic cross sections is studied in detail with a semiclassical analysis, and a comparison is made with previous calculations. The vibrational energies for several different X²Π bound potential functions for OH are also calculated and compared with published results. © 1999 Published by Elsevier Science Ltd. All rights reserved.

1. Introduction

The energization of H and D by collisions with energetic oxygen atoms is an important process with regard to the nonthermal escape of H and D from Mars and Venus. Translationally energetic oxygen atoms are produced from dissociative recombination of O₂⁺, that is, O₂⁺ + e → O + O with several different channels depending on the electronic states of the product oxygen atoms (Shizgal and Arkos, 1996; Cooper et al., 1984; Gurwell and Yung, 1993). This reaction is followed by translational energy transfer in collisions of oxygen atoms with H and D, and energization of H and D above the escape velocity of the planets. The accurate collision dynamics of O–H and O–D collisions are required in order to provide reliable estimates of the efficiency of this energization process leading to enhanced escape of H and D. This process was studied by Cooper et al. (1984) some time ago and recently by Gurwell and Yung (1993). Hodges (1993) recalculated the O–H and O–D collision cross sections and obtained different results from that obtained by Cooper et al. (1984). A major objective of the present paper is to re-examine the O–H potential functions and to attempt to resolve the different results reported by

Cooper et al. (1984) and by Hodges (1993). Some of these potential functions have been recently updated by Pradhan (1995) and Nemukhin and Grigorenko (1997). The kinetic theory of the energization process and the determination of the velocity distribution functions of energized H and D is presented in a subsequent publication.

The OH radical plays a very important role in the aeronomy of the Earth (Crosley, 1997; Vandop and Krol, 1996; Makhlouf et al., 1995; Lopezgonzalez et al., 1996) and other planets (Ip, 1997), in the development of diagnostic techniques for interstellar clouds (Szymczak and Lesqueren, 1995) and comets (Meech and Weaver, 1996), in astrophysics (Oneal and Neff, 1997), as well as the quantum behaviour of OH in different molecular environments (Wright and Donaldson, 1985), photoassociation (Korolkov et al., 1996) and in electron–OH scattering (Chen and Morgan, 1997). Accurate O–H potential functions are clearly important input data for numerous applications. In addition to the calculation of the scattering cross sections, the OH vibrational states in the ground X²Π state are determined with the Quadrature Discretization Method (QDM) described in recent papers (Shizgal and Chen, 1996; Shizgal, 1997).

In Section 2, the details of the four interaction potentials are presented and discussed. The recent calculations reported by Nemukhin and Grigorenko (1997) and the unpublished work by Pradhan (1995) are also included. A detailed analysis of the scattering cross sections for

¹Permanent Address: Department of Chemistry and Department of Earth and Ocean Sciences, University of British Columbia, Vancouver, British Columbia, Canada V6T 1Z1.

Table 1
The X²Π potentials

<i>r</i>	P	<i>r</i>	NG	<i>r</i>	LVWD	<i>r</i>	
1.00	11.667	1.00	11.667	1.00	11.667	0.90	9.91
1.10	6.138	1.10	6.138	1.10	6.138	1.00	6.26
1.20	2.293	1.20	2.293	1.20	2.293	1.10	3.57
1.25	0.84723	1.25	0.84723	1.25	0.84723	1.20	1.25
1.30	-0.47118	1.30	-0.47118	1.30	-0.39900	1.30	-0.57
1.50	-3.37316	1.50	-3.37316	1.50	-3.28700	1.40	-1.80
1.60	-4.05089	1.61	-3.97575	1.75	-4.41200	1.50	-2.88
1.75	-4.50268	1.70	-4.31208	1.83	[-4.47100]	1.60	-3.59
1.90	[-4.53042]	1.75	-4.40487	2.00	-4.32700	1.70	-3.84
2.00	-4.40562	1.80	-4.46228	2.25	-3.77100	1.85	[-4.04]
2.10	-4.20861	1.83	[-4.47616]	2.50	-3.10000	1.95	-3.97
2.25	-3.83143	1.89	-4.46038	2.75	-2.41600	2.00	-3.89
2.40	-3.40631	1.98	-4.35807	3.00	-1.81200	2.20	-3.48
2.50	-3.11515	2.08	-4.18637	3.25	-1.31600	2.40	-3.05
2.75	-2.40954	2.36	-3.45358	3.50	-0.93100	2.60	-2.53
3.00	-1.78479	2.55	-2.90719	3.75	-0.64700	2.80	-2.07
3.25	-1.26939	2.65	-2.63889	4.00	-0.44400	3.00	-1.66
3.50	-0.87085	2.74	-2.38012	4.50	-0.20700	3.20	-1.28
3.75	-0.58078	2.83	-2.13305	5.00	-0.09200	3.40	-0.98
4.00	-0.38062	3.02	-1.68298	5.50	-0.03099	3.60	-0.74
4.50	-0.16135	3.31	-1.13142	6.00	-0.01405	3.80	-0.54
4.75	-0.10566	3.50	-0.84761	7.00	-0.00271	4.00	-0.41
5.00	-0.06970	3.78	-0.53551	7.10	-0.00196	4.20	-0.30
5.25	-0.04632	3.97	-0.39047	7.20	-0.00179	4.40	-0.22
5.50	-0.03099	4.25	-0.24272			4.60	-0.16
6.00	-0.01405	4.72	-0.11238			4.80	-0.11
7.00	-0.00271	5.67	-0.02966			5.00	-0.08
7.10	-0.00196	7.56	-0.00816			5.20	-0.05
7.20	-0.00179	9.45	-0.00653			5.40	-0.03
		9.60	-0.00321			6.00	-0.00538
		9.70	-0.00301			6.10	-0.00487
		9.80	-0.00283			6.20	-0.00442

r is in atomic units and the energies in eV. P, NG, LVWD, and H correspond to results by Pradhan (1995), Nemukhin and Grigorenko (1997), van Dishoeck et al. (1983) and Hodges (1993), respectively.

these potentials is presented in Section 3. Section 4 reports on the results of the calculation of the bound vibrational states in OH and OD.

2. O–H interaction potentials

The collision dynamics of O–H is determined from the four interaction potentials X²Π, ²Σ⁻, ⁴Π and ⁴Σ⁻ calculated some time ago by Langhoff et al. (1982), van Dishoeck et al. (1983) and van Dishoeck and Dalgarno (1983). Pradhan (1995) recalculated the potential curves for the X²Π and ²Σ⁻ states, and some other states. Nemukhin and Grigorenko (1997) recently reported results for the X²Π as well as several other states. The radial variation of the X²Π state from these different sources is shown in Table 1 and Fig. 1. The entries in the table denoted by P and NG are the numerical values provided to the author by Pradhan (1995), and by Nemukhin and Grigorenko (1997), respectively. The values of Langhoff

et al. (1982) (denoted by LVWD) are from Table V in their paper which are similar to the values in Table I in the paper by van Dishoeck et al. (1983). The last column in Table 1 (labelled H) are the values taken from the curve in Fig. 1 of the paper by Hodges (1993) (adapted from the paper by van Dishoeck et al. (1983)). In each case, the energies are listed relative to the energy of the separated atoms taken as the energy for the largest *r* value in the relevant table or figure.

The solid curve in Fig. 1 is used as a reference to compare the different potentials, and is given by the generalized Morse potential from Wright and Donaldson (1985) of the form,

$$V(r) = D_e [1 - e^{-\beta x}]^2, \quad x = r - r_e \quad (1)$$

and

$$\beta = \beta_0 (1 + \lambda_1 x + \lambda_2 x^2), \quad (2)$$

with $r_e = 1.8324$ atomic units (au), $D_e = 4.582$ eV,

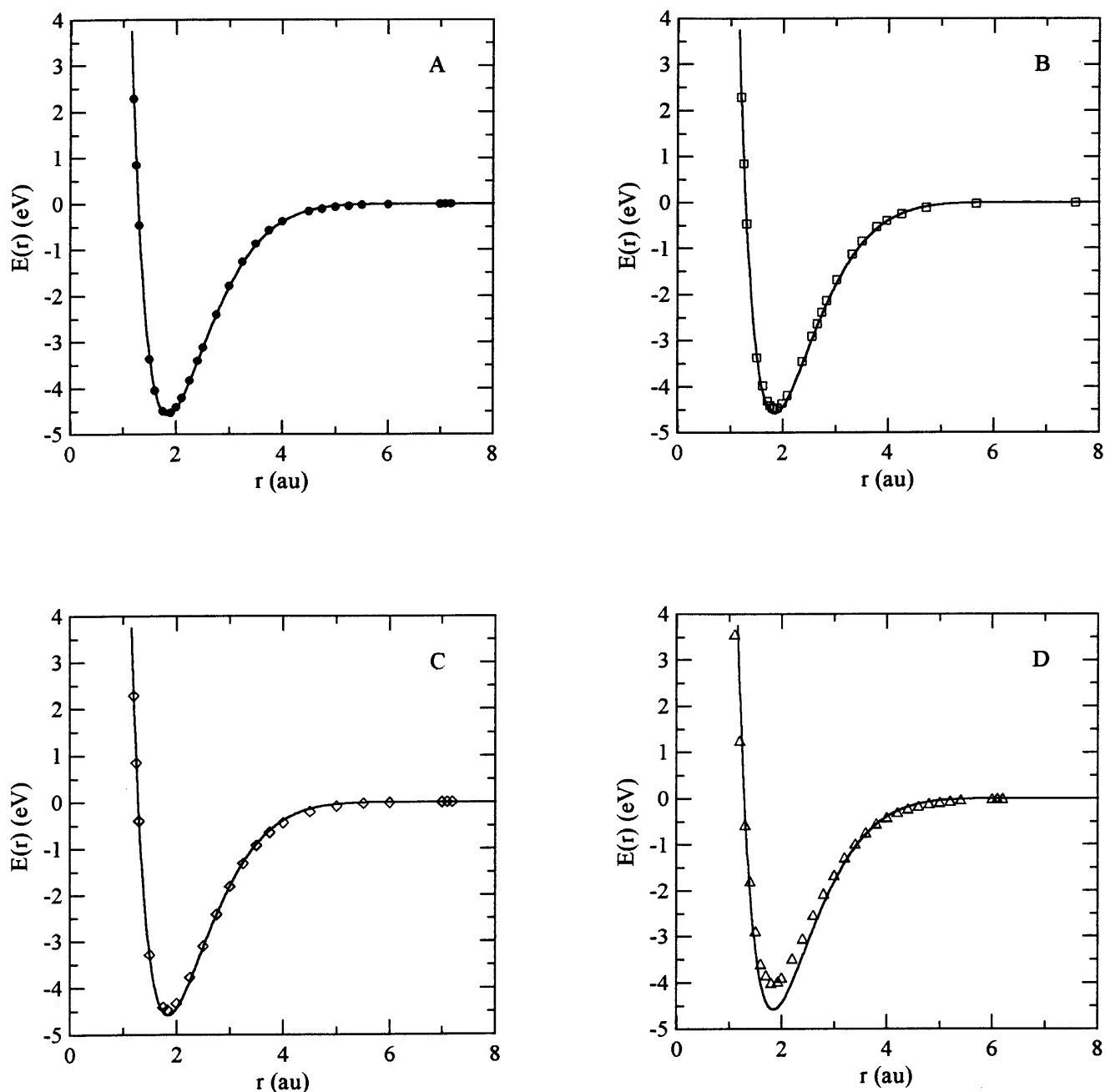


Fig. 1. Radial variation of the bound $X^2\Pi$ potential. The solid line in each figure is the generalized Morse potential of eq. (1) and eq. (2). (A) filled circle; Pradhan (1995), (B) open square, Nemukhin and Grigorenko (1997); (C) open diamond, Langhoff et al. (1982); (D) open triangle, Hodges (1993).

$\beta_0 = 1.239$, $\lambda_1 = 0.001$ and $\lambda_2 = 0.037$. For clarity, each set of data in Table 1 is compared separately in each of the four figures of Fig. 1. There are only subtle differences between these potentials and the modified Morse potential, except for the potential by Hodges. The well depth for this potential is shallower and not in agreement with the others. The minima for each potential is indicated by the square brackets in Table 1. The repulsive parts of the potentials appear to be well approximated by this generalized Morse potential so that the values for the

first four entries in Table 1 are the values obtained with eq. (1) and eq. (2), and are shown in italics in the table.

The large r asymptotic behaviour of the potentials is shown in Fig. 2 in comparison with the asymptotic form of the Π state (short dashed curve) by Miller and Kelley (1973) given by,

$$V_{\text{asy}}^{(\Pi)}(r) \approx -\frac{250.9}{r^6}, r \rightarrow \infty \quad (3)$$

with r in au and $V_{\text{asy}}^{(\Pi)}(r)$ in eV. The entries in Table 1 in

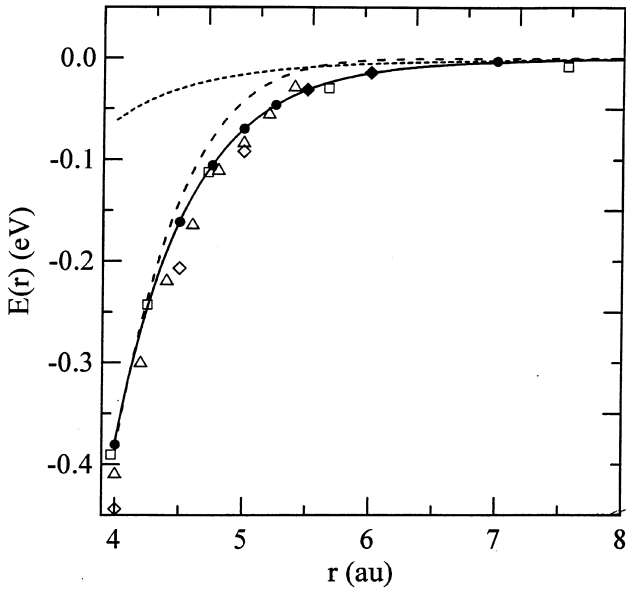


Fig. 2. Radial variation of the long range portion of the bound $^2\Pi$ potential. The solid line is the spline fit to the data by Pradhan (1995); the short dashed line is the asymptotic result given by eq. (3); the long dashed line is the generalized Morse potential of eq. (1) and eq. (2). The symbols are defined in the caption to Fig. 1.

bold type are the asymptotic energies given by eq. (3). Further details of Fig. 2 are discussed later.

The asymptotic behaviour of the potentials is very important in the calculation of the elastic scattering cross sections, as will be demonstrated later. Both Cooper et al. (1984) and Hodges (1993) do not specify exactly the way in which they merged their data at small r to the asymptotic result, eq. (3); see Table 1. The results by Langhoff et al. (1982) do not extend into the asymptotic region and the interpolation of the tabulated values and the asymptotic results is somewhat arbitrary. The same applies to the potential by Hodges (1993) which is adapted from van Dishoeck et al. (1983) but differs significantly from theirs, particularly with respect to the shallower well.

In order to get complete potentials for all r , the numerical data were extended to include the asymptotic regions. The procedure to accomplish this in this paper is as follows. The energies calculated from eq. (3) were subtracted from the energies by Pradhan (1995) in Table 1 for $r = 3.75\text{--}5.00$ au. The semilogarithmic plot of this energy difference was found to vary linearly with radial distance remarkably well. Moreover, the extrapolation into the region $r > 5$ au reproduced the values in the table extremely accurately. Therefore, for $r > 4.5$ au, the energies for this state are given by

$$V^{(2\Pi)}(r) = -381.6e^{-1.772r} - \frac{250.9}{r^6}, r \geq 4.5 \text{ au} \quad (4)$$

with r in au and $V^{(2\Pi)}(r)$ in eV. The constants in the

exponential function are the result of the fitting procedure and are empirical. The use of the data from Nemukhin and Grigorenko (1997) provides a similar excellent exponential fit, but with different constants. The approach into the asymptotic region is therefore very gradual and eq. (3) gives the interaction energy only for $r \approx 8\text{--}10$ au. The final potential adopted here is then the numerical values in Table 1 reported by Pradhan (1995) up to $r = 4.5$ au and the analytic fit given by eq. (4) beyond 4.5 au.

The solid line in Fig. 2 is the spline fit to the tabulated values for $r \leq 4.5$ au and the analytic fit, eq. (4), for $r > 4.5$ au. The table used for the spline fit is augmented with several values for $r > 4.5$ au calculated with eq. (4). The long dashed curve in Fig. 2 is the generalized Morse potential given by eq. (1) and eq. (2). The values of the potentials by Pradhan (1995) (filled circles) and by Nemukhin and Grigorenko (1997) (open squares) are in good agreement. These potentials are available to sufficiently large r so that a useful comparison can be made with the asymptotic result, eq. (3). The results by Pradhan (1995) appear to be consistent with the asymptotic behaviour of eq. (3). The results by Nemukhin and Grigorenko (1997) appear somewhat below the asymptotic values. However, it is not known at what radial distance the asymptotic behavior of eq. (3) becomes accurate.

The numerical values for the energies of the $^2\Sigma^-$ state for three different sources are listed in Table 2 and shown in Fig. 3(A). These three sets of data were provided by Pradhan (1995) denoted by P, obtained from Table 1 from the paper by van Dishoeck et al. (1983) labelled VLD, and adapted from Figure 1 in the paper by Hodges (1993) labelled H (the source of which is van Dishoeck et al. (1983)). For the $^2\Sigma^-$ states, the asymptotic behaviour is given by

$$V_{\text{asy}}^{(2\Sigma)}(r) \approx \frac{248.4}{r^6}, r \rightarrow \infty, \quad (5)$$

with r in au and $V_{\text{asy}}^{(2\Sigma)}(r)$ in eV. The behaviour of these different potentials in comparison with the asymptotic behaviour (dashed curve) is shown in Fig. 3(B). The difference between the tabulated values in Table 2 by Pradhan (1995) and this asymptotic behaviour was fitted to an exponential for the four points $r = 4.50\text{--}5.25$ au. Therefore, for $r \geq 5.25$ au, the energies of this state are given approximately by

$$V^{(2\Sigma^-)}(r) = 764.9e^{-2.0289r} + \frac{248.4}{r^6}, r \geq 5.25 \text{ au} \quad (6)$$

with r in au and $V^{(2\Sigma^-)}(r)$ in eV. This analytic fit gives values of the potential which are slightly above the energies at 6 au and 7 au in Table 2.

Results for the relevant quartic states are those reported by van Dishoeck and Dalgarno (1983) in Fig. 6

Table 2
The ${}^2\Sigma^-$ potentials

r	P	r	VLD	r	H
1.60	4.61855	1.50	5.60	1.05	11.81
1.75	3.79385	1.75	3.88	1.10	10.59
1.90	3.29936	1.83	3.57	1.20	9.39
2.00	3.04831	2.00	1.34	1.30	7.51
2.10	2.81720	2.25	2.51	1.40	6.37
2.25	2.47489	2.50	1.92	1.50	5.44
2.40	2.13463	2.75	1.43	1.60	4.71
2.50	1.91633	3.00	1.03	1.70	4.08
2.75	1.42829	3.25	0.73	1.80	3.65
3.00	1.04019	3.50	0.52	1.90	3.32
3.25	0.74538	3.75	0.37	2.00	3.08
3.50	0.52700	4.00	0.25	2.20	2.59
3.75	0.36781	4.50	0.12	2.40	2.10
4.00	0.25325	5.00	0.05	2.60	1.69
4.50	0.11508			2.80	1.28
4.75	0.07585			3.00	0.95
5.00	0.04913			3.20	0.71
5.25	0.03120			3.40	0.54
5.50	0.01935			3.60	0.38
6.00	0.00677			3.80	0.30
7.00	0.00034			4.00	0.22
				4.20	0.14
				4.40	0.11
				4.60	0.08

r is in atomic units and the energies in eV. P, VLD and H correspond to the results by Pradhan (1995), van Dishoeck et al. (1983) and Hodges (1993), respectively.

of their paper. This is the source for the potentials used by Cooper et al. (1984) and by Hodges (1993). The numerical values for these potentials were obtained from this figure as well as Fig. 1 of Hodges (1993) and Fig. 1 of Cooper et al. (1984). The numerical values from the digitization of the graphical data in these references are shown in Tables 3 and 4, and labelled VD, H and CYD for van Dishoeck and Dalgarno (1983), Hodges (1993) and Cooper et al. (1984), respectively. The energies are all in eV and relative to the zero of energy for the separated atoms. Reasonable agreement is found for the potentials shown in Tables 3 and 4 employed by Hodges (1993) and reported by van Dishoeck and Dalgarno (1983). However, the data reported by Cooper et al. (1984) for both the ${}^4\Sigma^-$ and ${}^4\Pi$ states are significantly lower in the important region beyond about 2.2 au. It is unfortunate that numerical data for these potentials is not available. The potentials listed in the tables determined from the graphical data reported in the references cited is believed to be accurate to ± 0.05 eV. The errors can be large for small r where the potentials vary rapidly with r , and as well as for large r where the energy reported is determined by subtracting the asymptotic values.

The asymptotic dependence of the quartic states was determined as for the doublet states. The asymptotic energies, eq. (3) and eq. (5) were subtracted from the

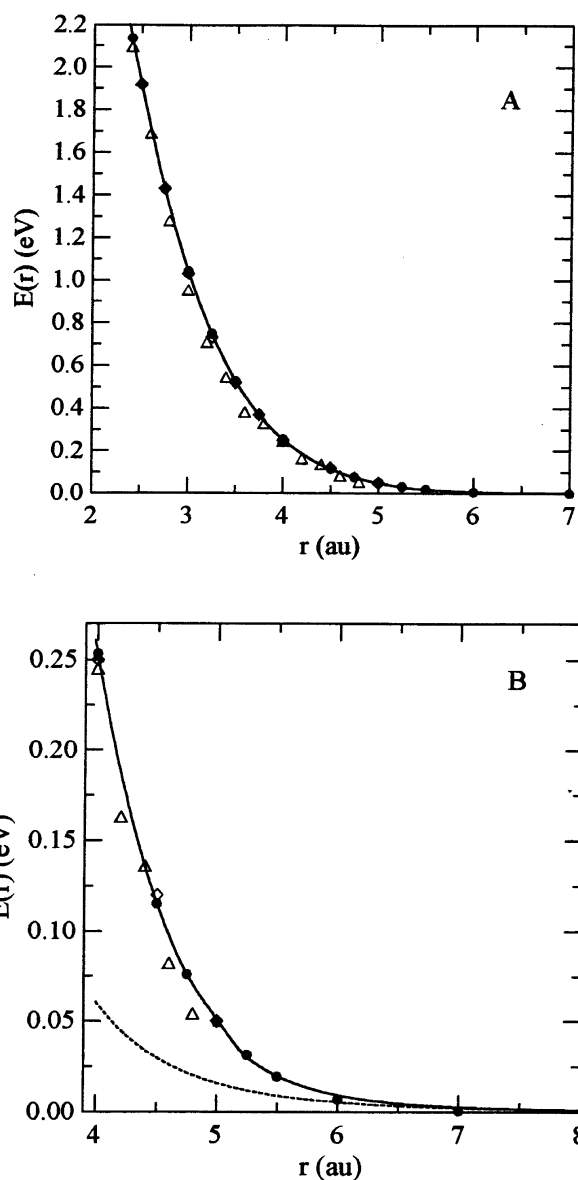


Fig. 3. (A) The radial variation of the ${}^2\Sigma^-$ potential. The solid line is the spline fit to the data by Pradhan (1995). (B) Asymptotic behaviour of the ${}^2\Sigma^-$ potential. The short dashed line is the asymptotic result given by eq. (5); filled circle, Pradhan (1995); open square, Nemukhin and Grigorenko (1997); (C) open diamond, van Dishoeck et al. (1983); (D) open triangle, Hodges (1993).

results by van Dishoeck and Dalgarno (1983) in Tables 3 and 4, and the difference was fitted to exponential functions. The four data points $r = 3.8$ – 4.4 au were used and the analytic forms that were found are

$$V^{(4\Pi)}(r) = 171.1e^{-1.641r} + \frac{250.9}{r^6}, r \geq 4.2 \text{ au} \quad (7)$$

and

$$V^{(4\Sigma^-)}(r) = 104.2e^{-1.755r} + \frac{248.4}{r^6}, r \geq 4 \text{ au} \quad (8)$$

Table 3
The ${}^4\Sigma^-$ potential

r	VD	H	CYD
1.50	5.02	5.01	4.91
1.60	4.26	4.22	4.17
1.70	3.68	3.57	3.55
1.80	3.28	3.13	3.09
1.90	2.87	2.80	2.68
2.00	2.52	2.56	2.33
2.10	2.23	2.29	2.06
2.20	2.00	2.01	1.78
2.30	1.75	1.79	1.50
2.40	1.58	1.55	1.29
2.50	1.40	1.36	1.05
2.60	1.23	1.20	0.86
2.70	1.08	1.03	0.71
2.80	0.97	0.90	0.57
3.00	0.70	0.68	0.41
3.20	0.52	0.49	0.26
3.40	0.39	0.35	0.17
3.60	0.30	0.27	0.10
3.80	0.21	0.19	0.07
4.00	0.16	0.14	0.05
4.20	0.11	0.11	0.04
4.40	0.08	0.09	0.03
4.60	0.05	0.08	0.01

r is in atomic units and the energies in eV. VD, H and CYD denote the potentials employed by van Dishoeck and Dalgarno (1983), Hodges (1993) and Cooper et al. (1984), respectively. The energies are in eV relative to the ground level.

Table 4
The ${}^4\Pi$ potential

r	VD	H	CYD
2.00	5.44	5.41	5.32
2.10	5.32	5.22	4.72
2.20	4.70	4.68	4.15
2.30	4.03	4.08	3.60
2.40	3.49	3.54	3.15
2.50	2.93	2.94	2.68
2.60	2.62	2.50	2.32
2.70	2.24	2.12	2.00
2.80	1.98	1.85	1.76
2.90	1.65	1.58	1.50
3.00	1.39	1.39	1.28
3.20	1.05	1.03	0.88
3.40	0.79	0.76	0.60
3.60	0.58	0.60	0.43
3.80	0.42	0.41	0.31
4.00	0.30	0.33	0.21
4.20	0.22	0.22	0.16
4.40	0.16	0.14	0.09
4.60	0.10	0.08	0.07
5.00	0.03	0.05	0.05

r is in atomic units and the energies in eV. VD, H and CYD denote the potentials employed by van Dishoeck and Dalgarno (1983), Hodges (1993) and Cooper et al. (1984), respectively.

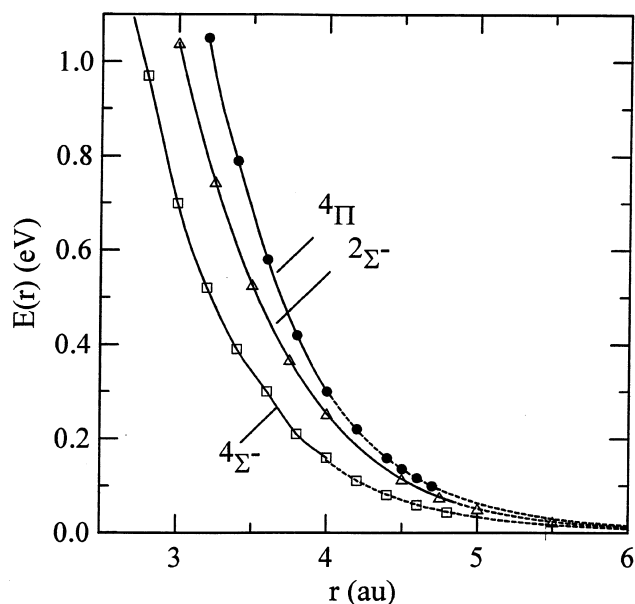


Fig. 4. Comparison of the radial variation of the repulsive potentials, ${}^4\Sigma^-$ (open square), ${}^2\Sigma^-$ (open triangle) and ${}^4\Pi$ states (filled circle). The solid lines are the spline fits to the data in the second columns of Tab. 1, Tab. 2 and Tab. 3. The dashed lines are the asymptotic fits given by eq. (6), eq. (7) and eq. (8).

with r in au and $V(r)$ in eV. Figure 4 shows the radial variation of the three repulsive states over the region that contributes most to the scattering for energies of the order of 1 eV. The solid lines are the spline fits to the values in the tables augmented with several data entries from the analytic fits, eqs. (6–8). The dashed lines are the asymptotic values given by eqs. (6–8). The potentials employed in this paper are of longer range than those used by Cooper et al. (1984) and by Hodges (1993) and approach the $1/r^6$ behaviour more slowly. Without more detailed quantum calculations of the asymptotic forms of these potentials, the merging of the tabulated values with the asymptotic variations, eq. (3) and eq. (5), remains subjective.

The four potentials employed in the present work to study O–H and O–D scattering are the $X^2\Pi$ state by Pradhan (1995) in the second column in Table 1, the ${}^2\Sigma^-$ state by Pradhan (1995) in the second column of Table 2, the ${}^4\Sigma^-$ and ${}^4\Pi$ states by van Dishoeck and Dalgarno (1983) and listed in the second columns of Tables 3 and 4, respectively. These tabulated values are augmented with the analytic fits given by eq. (4) and eqs. (6–8) as discussed. The data in Tables 1–4 obtained by digitizing graphical data in the references cited are believed to be within $\pm 5\%$ of the data used to plot the graphs. Two numerical potentials digitized independently from the same graph were within 2% of each other as were the cross sections calculated with the potentials.

3. Scattering cross sections

The elastic scattering cross sections for O–H and O–D collisions for each of the four interaction potentials, $V^{(j)}(r)$, of Section 2 were calculated quantum mechanically. The details of the calculation were described by Hodges (1993) and Cooper et al. (1984) and also appear in standard references (Bernstein, 1966; Rodberg and Thaler, 1967). The differential cross section, $\sigma(E, \theta)$ at relative energy E and scattering angle θ is given by the sum of the cross sections for each potential weighted with the statistical weight of the j th channel

$$\sigma(E, \theta) = \sum_{j=1}^4 g_j |f_j(E, \theta)|^2, \quad (9)$$

where $f_j(E, \theta)$ is the scattering amplitude for the j th channel expressed in terms of the scattering phase shifts, $\delta_l^{(j)}$,

$$f_j(E, \theta) = \frac{1}{2ik} \sum_{l=1}^{\infty} (2l+1) \times [\exp(2i\delta_l^{(j)}) - 1] P_l(\cos \theta). \quad (10)$$

In eq. (10), $P_l(\cos \theta)$ are the Legendre polynomials, $k = \sqrt{2\mu E}/\hbar$ is the wave number, and μ is the reduced mass equal to 0.94826 amu for O–H and 1.7904 amu for O–D. The phase shifts are determined in the usual way by numerically solving the radial Schroedinger equation,

$$\frac{d^2 u_l^{(j)}(r)}{dr^2} + [k^2 - U_{\text{eff}}^{(j)}] u_l^{(j)}(r) = 0, \quad (11)$$

where $U_{\text{eff}}^{(j)}(r) = U^{(j)}(r) + l(l+1)/r^2$ and $U^{(j)}(r) = 2\mu V^{(j)}(r)/\hbar^2$. The phase shifts are determined from the asymptotic form of the radial wavefunction given by

$$u_l^{(j)}(r) \approx \frac{1}{kr} \sin \left(kr - l\frac{\pi}{2} + \delta_l^{(j)} \right), r \rightarrow \infty. \quad (12)$$

An alternate and often very accurate method for calculating the phase shifts is the Wentzel–Kramers–Brillouin (WKB) semiclassical approximation (Cohen, 1978; Kennedy and Smith, 1967), given by

$$\delta_l^{(j)} = \frac{l+1/2}{2} \pi - kr_0^{(j)} + \int_{r_0^{(j)}}^{\infty} [k_l^{(j)}(r) - k] dr, \quad (13)$$

where

$$k_l^{(j)}(r) = \sqrt{k^2 - U_{\text{eff}}^{(j)}(r)}. \quad (14)$$

In eq. (13) and eq. (14), $r_0^{(j)}$ is the classical turning point for which $k^2 = U_{\text{eff}}^{(j)}(r_0^{(j)})$. The WKB approximation is computationally faster than the quantum approach, but in addition it provides a useful physical interpretation of the scattering, which is the principal use in this paper. The quantum mechanical scattering phase shifts for each of the four potentials from 0.01 eV to 5 eV were calculated as done previously by Cooper et al. (1984) and Hodges (1993). The total cross sections for each independent channel are given by

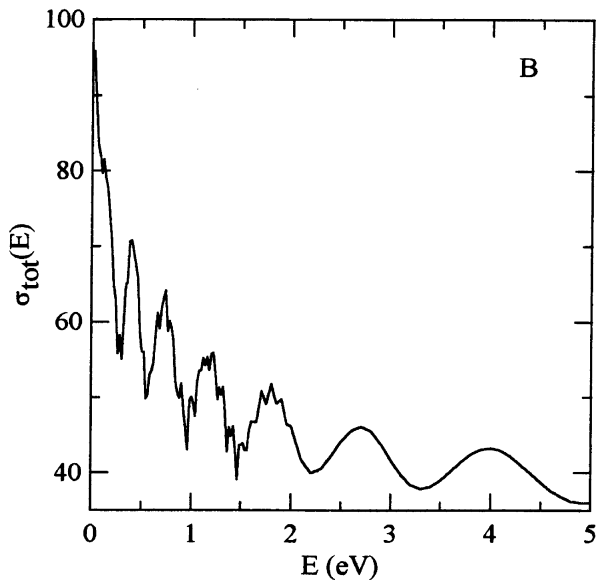
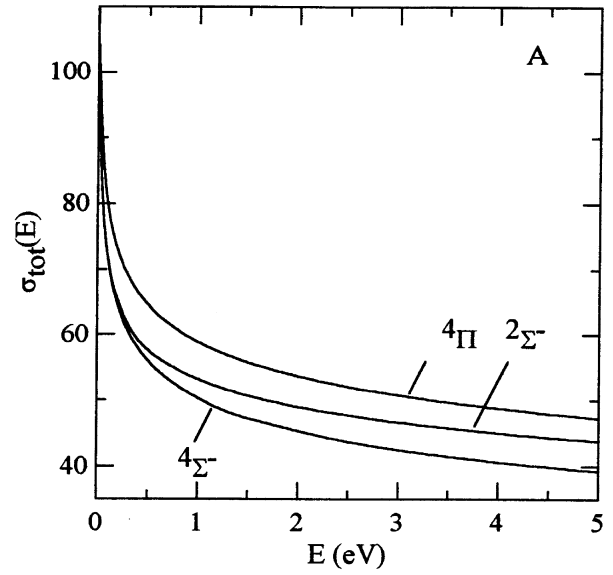


Fig. 5. Energy variation of the total elastic O–H cross sections in \AA^2 . (A) Cross sections for the $4\Sigma^-$, $2\Sigma^-$ and 4Π states; (B) Cross section for 2Π state.

$$\sigma_{\text{tot}}^{(j)}(E) = 2\pi \int_0^{\pi} \sigma^{(j)}(E, \theta) \sin(\theta) d\theta. \quad (15)$$

The present calculations give the energy variation of the total cross sections shown in Fig. 5(A). The ordering of the cross sections for the three repulsive states $\sigma_{\text{tot}}^{(4\Sigma^-)} < \sigma_{\text{tot}}^{(2\Sigma^-)} < \sigma_{\text{tot}}^{(4\Pi)}$ shown in Fig. 5(A) is entirely consistent with the order of the potentials in Fig. 4. The choice of points in the determination of the analytic expressions, eq. (4) and eqs. (6–8) is somewhat arbitrary. Several other expressions were used and these gave total cross sections that differed from those in Fig. 5(A) by $\pm(3-5)\%$. The cross section from the bound 2Π state is

shown in Fig. 5(B). The oscillations in this cross section can be related to the bound states in the potential.

Hodges (1993) reported identical total cross sections for the $^2\Sigma^-$ and $^4\Sigma^-$ states, whereas Cooper et al. (1984) show a considerable difference in the total cross sections for these two potentials. As shown in Fig. 4, the $^4\Sigma^-$ state is somewhat below the $^2\Sigma^-$ state. It does not appear reasonable that the cross sections for these two potentials are identical. Nor is it reasonable that the cross sections should differ as much as shown in Figure 4 in the paper by Cooper et al. (1984). For the $^2\Sigma^-$ state, Hodges (1993) and Cooper et al. (1984) report a cross section that varies from 38 to 45 \AA^2 in the energy range 1–5 eV. The present results give a cross section from 44 to 53 \AA^2 which is about 15% larger. Cooper et al. (1984) report a cross section for the $^4\Sigma^-$ state that varies slowly from 23 to 26 \AA^2 whereas the present results give a cross section that varies from 39 to 50 \AA^2 which is significantly larger. Cooper et al. (1984) report a cross section for the $^4\Pi$ state that is greater than the cross section for the $^2\Sigma^-$ state which is unreasonable, as noted by Hodges (1993). Hodges (1993) reports a cross section for this state that varies from approximately 46 to 57 \AA^2 in reasonable agreement with the present results which are from 47 to 59 \AA^2 . A detailed comparison of the results for the cross section for the $^2\Pi$ state was not carried out but it is clear that there are significant differences. The present results show maxima in the cross section at 1.2, 1.8, 2.7 and 4.0 eV, with cross section values of 56, 52, 46 and 43 \AA^2 , respectively. The results by Cooper et al. (1984) are similar but not in complete agreement with maxima at about 0.9, 1.5, 2.2 and 3.3 eV, and cross section values of approximately 50, 43, 44, and 40 \AA^2 , respectively. Hodges (1993) shows 5 rather than 4 maxima at about 1.0, 1.4, 2.2, 3.2 and 4.8 eV, with cross section values of approximately 68, 66, 62, 58, and 56 \AA^2 , respectively.

In order to explain the different results, in particular for the repulsive potentials, two model potentials were constructed for the $^2\Sigma^-$ state as shown in Fig. 6. These correspond to different schemes for merging the tabulated values of the potentials with the asymptotic behaviour shown by the thin solid line. The two model potentials are denoted by long and short dashed curves and the actual potential used in this paper is shown as the bold solid curve. These model potentials are not unreasonable interpolations of the short and long range forms of the potential in view of the fact that the potentials available to Cooper et al. (1984) and Hodges (1993) are not well known beyond about 4–5 au. The recent calculations by Pradhan (1995) provide a much better result up to 7 au for the $^2\Pi$ and the $^2\Sigma^-$ states.

The WKB method was used to study the details of the scattering from the three potentials in Fig. 6 for $E = 1$ eV. The results are shown in Fig. 7. Figure 7(A) shows the variation of the classical turning points over the range of l values for which there are significant differences. The

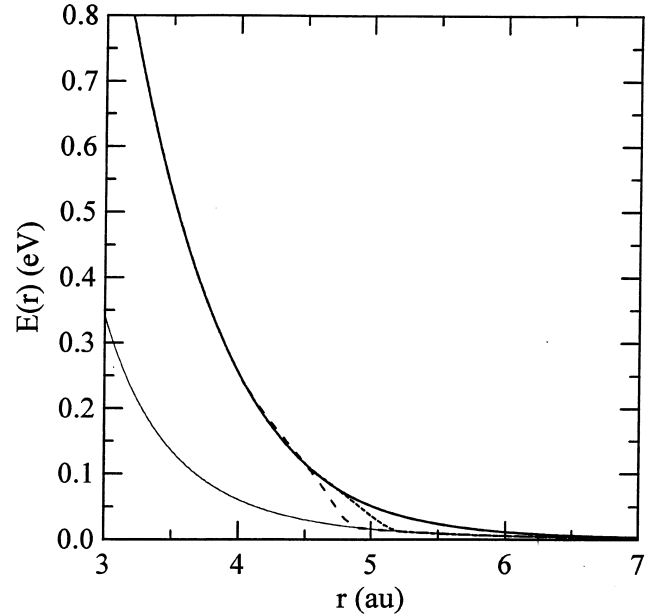


Fig. 6. Model potentials for the $^2\Sigma^-$ state are shown in short and long dashed lines. The solid light curve is the asymptotic result given by eq. (5). The solid dark line is the spline fit to the data by Pradhan (1995) listed in Tab. 1 including the data points given by eq. (6) for $r > 4.5$ au. The two additional dash curves are model potentials with arbitrary extrapolations to the asymptotic result.

differences arise directly from the way each potential was made to merge with the asymptotic behaviour. The corresponding phase shifts are shown in Fig. 7(B), and the differences in the phase shifts are significant. Figure 7(C) shows the partial sums, up to $l = L_m$ in the calculation of the total cross section, that is, the partial cross section,

$$S(L_m) = \frac{4\pi}{k^2} \sum_{l=0}^{L_m} (2l+1) \sin^2(\delta_l^{(j)}). \quad (16)$$

The converged total cross section, given by

$$\sigma_{\text{tot}}^{(j)}(E) = \frac{4\pi}{k^2} \sum_{l=0}^{\infty} (2l+1) \sin^2(\delta_l^{(j)}), \quad (17)$$

can be divided into two parts, that is,

$$\sigma_{\text{tot}}^{(j)}(E) = \sigma_{rp}^{(j)}(E) + \sigma_{lr}^{(j)}(E), \quad (18)$$

where the first term represents the sum over the ‘random phase’ (rp) shifts, $l \leq l_m^{(j)}$, analogous to eq. (16), and the second term is the contribution from phase shifts with $l > l_m^{(j)}$ that are determined by the long range (lr) portion of the potential. The quantum phase shifts for small l with smaller classical turning points sample the short range portion of the potentials and are considered random (modulo 2π) (Bernstein, 1966). Therefore, one can replace $\sim \sin^2(\delta_l^{(j)})$ with the average value of 1/2 so that,

$$\sigma_{rp}^{(j)}(E) = \frac{2\pi}{k^2} (l_m^{(j)} + 1)^2 \quad (19)$$

In Fig. 7(C), the three potentials give for $l = 50$, almost

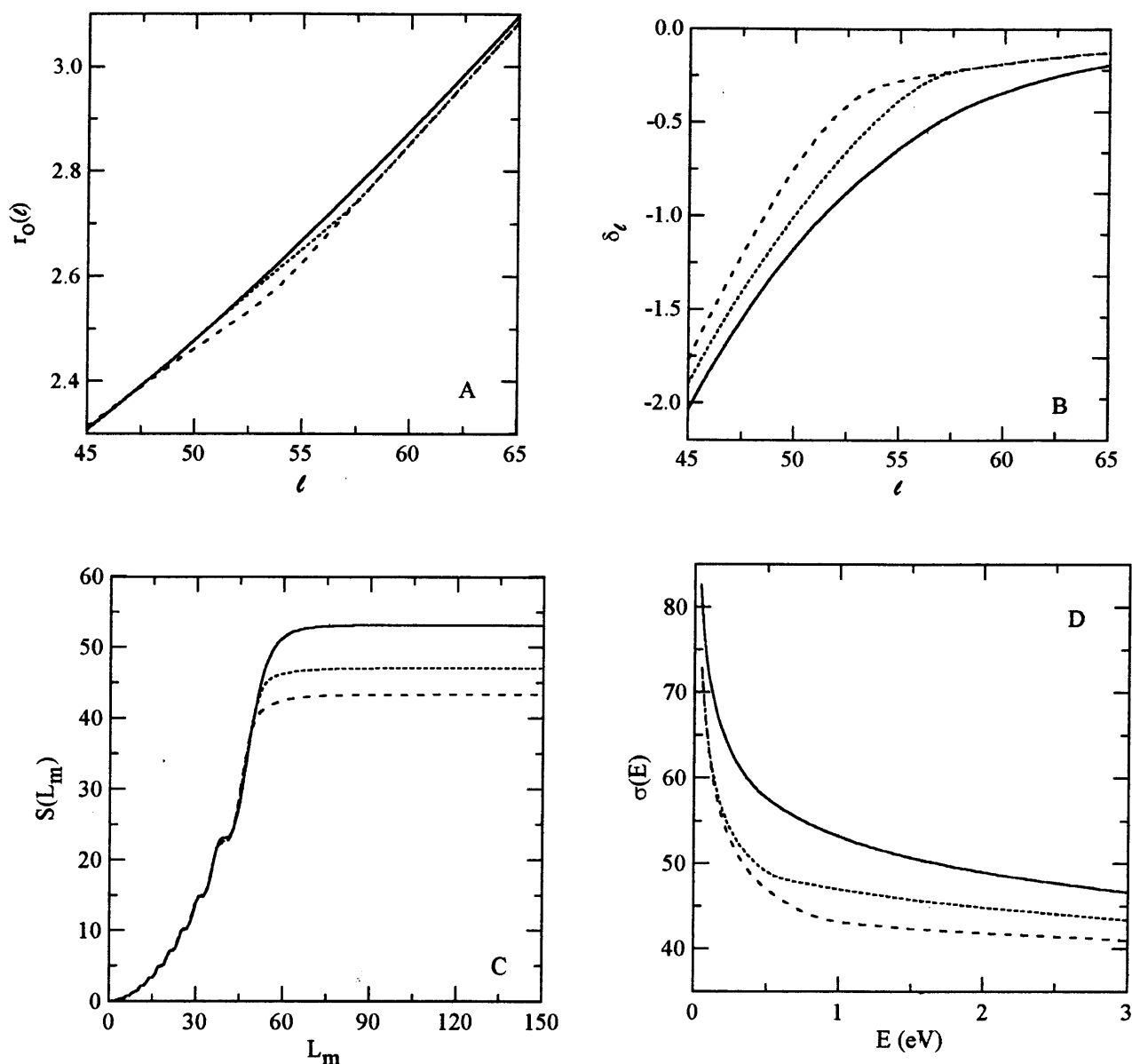


Fig. 7. A WKB analysis of the elastic scattering with $E=1$ eV. The dashed and solid lines correspond to potentials as shown in Fig. 6. (A) variation of the classical turning points (in au) with l ; (B) variation of the scattering phase shifts with l ; (C) variation of the partial sums (in \AA^2) in the calculation of the cross section with L_m , see eq. (16), and (D) the energy variation of the total cross sections (in \AA^2).

identical partial cross sections equal to 39.5, 40.6 and 40.4 \AA^2 , in the order of increasing range, respectively. With $l_m=50$ in eq. (19), the random phase cross section, at 1 eV, is 36.0 \AA^2 , which is in reasonable agreement considering that the number of phase shifts contributing is quite small and the semiclassical results are expected to be approximate. The remaining sum with $l>l_m$ is the contribution from the long range portion of the potential ($\sigma_{lr}^0(E)$) and for the three potentials these terms add an additional 3.8, 6.4 and 12.5 \AA^2 , respectively to σ_{rp}^0 . Therefore for these three potentials the contributions from the long range portion of the potentials to the total cross sections are 8.8%, 13.6% and 23.6%, respectively. It is

clear that the manner in which the short range tabulated potentials and long range behaviour are interpolated can significantly affect the cross sections. Since a much slower approach to the asymptotic region was adopted with the analytic results, eq. (4) and eqs. (6–8), the cross sections in this paper are larger than those reported by Hodges (1993). The bound $X^2\Pi$ state used by Hodges (1993) is too shallow (see Fig. 1) and the bound vibrational states calculated with this potential are not in agreement with published values as discussed in Section 4.

Figure 8(A) shows a representative differential cross section for the $^2\Pi$ state with $E=0.2$ eV. The quantum oscillations in the cross section and the sharp forward

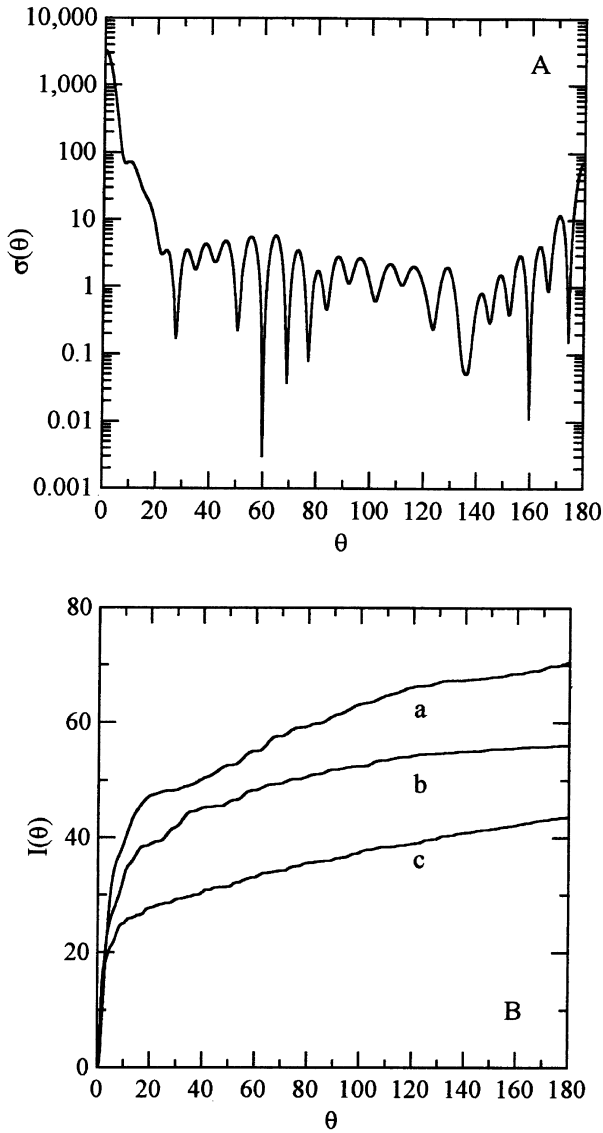


Fig. 8. (A) The differential cross section (in \AA^2) for O–H scattering for the $X^2\Pi$ state for $E=0.2$ eV; (B) The integrated cross section (in \AA^2), eq. (20), for energies (a) 0.2 eV, (b) 0.5 eV and (c) 1.5 eV.

scattering peak at small angles are characteristics of these differential cross sections. It is the small phase shifts that contribute to the scattering cross section at small angles and to the total cross section discussed in the previous paragraph. In subsequent kinetic theory calculations of the energization of H and D, the detailed structure of the differential cross sections should not be of importance, except for the peak at small angles. Cooper et al. (1984) reported the integrated cross sections, defined analogous to eq. (15), by

$$I^{(j)}(E, \theta) = 2\pi \int_0^\theta \sigma^{(j)}(E, \theta') \sin(\theta') d\theta'. \quad (20)$$

These integrated cross sections are shown in Fig. 8(B) for the $^2\Pi$ state at 0.2, 0.5 and 1.5 eV, respectively. Gurwell

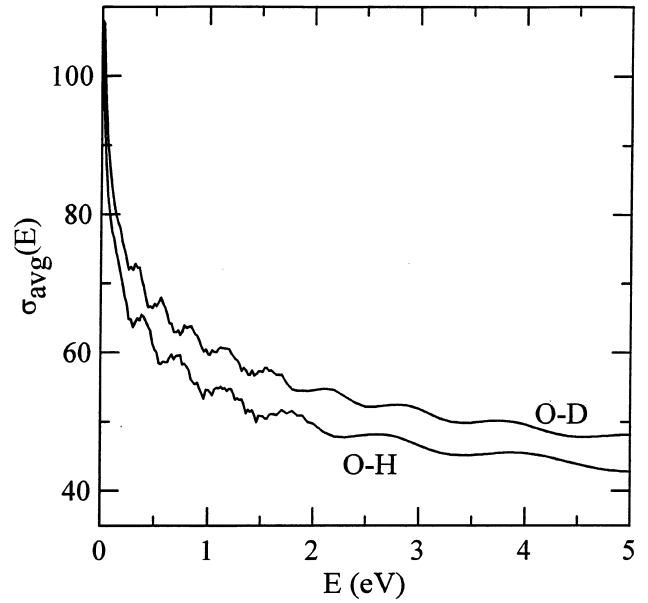


Fig. 9. Energy variation of the O–H and O–D elastic cross sections (in \AA^2) for the four potentials weighted with the appropriate statistical weight.

and Yung (1993) studied the energization of H and D using an analytic fit to such integrated cross sections and calculated the cross section by numerical differentiation. They did not use original scattering data but the result reported by Cooper et al. (1984) at one energy. It is clear from Fig. 8(B) that there is an important energy variation in the collision dynamics that should be taken into account.

The variation of the total cross sections summed over the contributions from each state and weighted appropriately is shown in Fig. 9 for O–H and O–D collisions. There is clearly a significant isotope effect. In their study of energization of H and D by energetic O, Gurwell and Yung (1993) assumed that the cross sections for O–H and O–D collisions are the same. It is clear that in any study of the differential escape of H and D should take account of the isotope effect in the differential cross sections.

4. Vibrational states

The vibrational energies for the $^2\Pi$ potential functions reported by Pradhan (1995), Nemukhin and Grigorenko (1997), Langhoff et al. (1982) and Hodges (1993) were also calculated as an additional comparison of these potential functions. The Quadrature Discretization Method (QDM) reported in recent papers (Shizgal and Chen, 1996; Shizgal, 1997) was used to determine the vibrational energies. The potentials used were those listed in Table 1 with a spline fit to interpolate within the table. The asymptotic energies are those given by eq. (3). Since the lower vibrational levels are considered, the asymptotic portion of the potential is not important in these

Table 5
The $^{16}\text{O}^1\text{H}$ vibrational energies

n	$E_n^{(\text{HH})}$	ΔE_n P	NG	LVWD	H
1	0.44260	0.00088	0.00432	0.00444	0.02509
2	0.86474	0.00154	0.01112	0.01390	0.06552
3	1.26680	0.00295	0.01879	0.02707	0.10387
4	1.64910	0.00598	0.02980	0.03990	0.12946
5	2.01190	0.01034	0.03990	0.05187	0.16382
6	2.35530	0.01571	0.04344	0.06482	0.20612
7	2.67960	0.02235	0.04964	0.08003	0.24939
8	2.98470	0.03076	0.06200	0.09776	0.29317
9	3.27030	0.04196	0.07760	0.11887	0.34245
10	3.53640	0.05733	0.09797	0.14452	0.39685

The first column lists the vibrational energies in eV given by Huber and Herzberg (1979). The other entries are the differences $\Delta E_n = E_n^{(\text{HH})} - E_n$. P, NG, LVWD and H correspond to results with the potentials by Pradhan (1995), Nemukhin and Grigorenko (1997), Langhoff et al. (1983) and Hodges (1993), respectively.

calculations. The potential in Table 1 from Pradhan (1995) with the asymptotic behaviour given by eq. (3), and the one with the asymptotic behaviour given by eq. (4) gave the same vibrational energies.

The QDM is based on a discrete representation of the Schroedinger equation,

$$-\frac{d^2\psi_n(x)}{dx^2} + U(x)\psi_n(x) = E_n\psi_n(x) \quad (21)$$

for the vibrational eigenfunction, $\psi_n(r)$, where $x = r_e - r$. A set of quadrature grid points, $\{x_{ij}\}$, are generated with a weight function, $w(x)$, derived from a Morse potential that approximates the potential considered. The vibrational energies are determined by the numerical diagonalization of the matrix representative of the Hamiltonian in this discrete basis, that is, the matrix

$$H_{ij} = \sum_{k=0}^N D_{ki} D_{kj} + [V(x_i) - \tilde{V}(x_i)]\delta_{ij}, \quad (22)$$

where

$$\tilde{V}(x) = \frac{1}{4} W^2(x) - \frac{1}{2} W'(x). \quad (23)$$

where $w(x) = \exp[\int_0^x W(x') dx']$ and D_{ij} is the QDM derivative matrix discussed in previous papers (Shizgal and Chen, 1996; Shizgal, 1997). The vibrational energies are determined from the numerical diagonalization of the matrix Hamiltonian defined by eq. (22).

Table 5 summarizes the results of these calculations. The vibrational energies calculated for the four different potentials are shown relative to the energies given by Huber and Herzberg (1979), in the column labelled $E_n^{(\text{HH})}$. The energies calculated with the four potential functions are all larger than the values given by Huber

and Herzberg (1979). The three lowest energies reported by Mélen et al. (1995) are 0.44267, 0.86481 and 1.26665 eV, respectively. As can be seen from the table, the potential by Pradhan (1995) gives the best agreement with the measured values, followed by the potential by Nemukhin and Grigorenko (1997). For the lower states, the potential by Langhoff et al. (1982) is comparable to these others but the differences get larger with increasing n . The results with the potential by Hodges (1993) (derived from the published data by Langhoff et al. (1982)) gives vibrational energies that are not in agreement with either the results obtained here with the potential by Langhoff et al. (1982) nor the measured values listed in Table 5.

5. Summary

In this paper, a detailed analysis of the four $X^2\Pi$, $^2\Sigma^-$, $^4\Pi$ and $^4\Sigma^-$ O–H potential functions reported in the literature has been provided together with an new interpolation of the short and long range portions of the potentials. The O–H and O–D quantum mechanical elastic scattering cross sections for these four potentials have been calculated and the isotope effect for the total cross sections has been reported. The isotope effect for the differential cross sections has an important role in the H and D nonthermal enhanced escape fluxes from Mars and Venus. The results differ from those reported by Cooper et al. (1984) and Hodges (1993) because of the different potential functions that were used, particularly their asymptotic variations. The $X^2\Pi$ potentials reported recently by Pradhan (1995) and Nemukhin and Grigorenko (1997) give good agreement with observed OH vibrational states. The present study demonstrates the need to have more precise quantum calculations of these interaction potentials.

Acknowledgements

This research is supported in part by a grant from the Natural Sciences and Engineering Research Council of Canada. I am pleased to acknowledge the assistance of Dr. Y. Shinagawa for arranging my visit to the Solar Terrestrial Environment Laboratory where this work was done. I am grateful to Professor A. V. Nemukhin for providing the data for the OH $X^2\Pi$ potential and to Dr. Atul D. Pradhan for his unpublished results for the $X^2\Pi$ and $^2\Sigma^-$ potentials.

References

- Bernstein, R.B. 1966. . Adv. Chem. Phys. 10, 75.
- Chen, X., Morgan, L.A., 1997. Low-energy electron scattering from the $X^2\Pi$ state of the OH molecule. J. Phys. B: At. Mol. Opt. Phys. 30, 3709–3717.

- Cohen, J.S., 1978. Rapid accurate calculation of JWKB phase shifts. *J. Chem. Phys.* 68, 1841–1843.
- Cooper, D.L., Yee, J.H., Dalgarno, A., 1984. Energy transfer in oxygen–hydrogen collisions. *Planet. Space Sci.* 32, 825–830.
- Crosley, D.R., 1997. 1994 tropospheric OH photochemistry experiment—a summary and perspective. *J. Geophys. Res.* 102, 6495.
- Fahr, H.J., Shizgal, B., 1983. Modern exospheric theories and their observational relevance. *Rev. Geop. Space Phys.* 21, 75–124.
- Gurwell, M.A., Yung, Y.L., 1993. Fractionation of hydrogen and deuterium on Venus due to collisional ejection. *Planet. Space Sci.* 41, 91–104.
- Hodges Jr., R.R., 1993. Collision cross sections and diffusion parameters for H and D in atomic oxygen. *J. Geophys. Res.* 98, 3799–3805.
- Huber, K. P. and Herzberg, G. (1979) *Molecular Spectra and Molecular Constants IV Constants of Diatomic Molecules*. Van Nostrand, New York.
- Ip, W.H., 1997. On the neutral cloud distribution in the Saturnian magnetosphere. *Icarus* 126, 47–57.
- Kennedy, M., Smith, F.J., 1967. The efficient computation of JWKB phase shifts. *Mol. Phys.* 13, 443–448.
- Korolkov, M.V., Manz, J., Paramonov, G.K., Schmidt, B., 1996. Vibrationally state-selective photoassociation by infrared sub-picosecond laser pulses: model simulations for $O+H\rightarrow OH(v)$. *Chem. Phys. Letters* 260, 604–610.
- Langhoff, S.R., van Dishoeck, E.F., Wetmore, R., Dalgarno, A., 1982. *J. Chem. Phys.* 77, 1379–1390.
- Lopezgonzalez, M.J., Murtagh, D.P., Espy, P.J., Lopezmoreno, J.J., Rodrigo, R., Witt, G., 1996. A model study of the temporal behaviour of the emission intensity and rotational temperature of the OH Mienel bands for high-latitude summer conditions. *Annales Geophysicae—Atmos. Hydrosph. Space Sci.* 14, 567–596.
- Makhlouf, U.B., Picard, R.H., Winick, J.R., 1995. Photochemical–dynamical modeling of the measured response of airglow to gravity waves. 1. Basic model for OH airglow. *J. Geophys. Res.—Atmos.* 100, 11289–11311.
- Meech, K.J., Weaver, H.A., 1996. Unusual comets (questionable) as observed from the Hubble space telescope source. *Earth Moon and Planets* 72, 119–131.
- Mélen, F., Sauval, A.J., Grevesse, N., Farmer, C.B., Cervais, Ch., Delbouille, L., Roland, G., 1995. A new analysis of the OH radical spectrum from solar infrared observations. *J. Molec. Spectrosc.* 174, 490–509.
- Nemukhin, A.V., Grigorenko, B.L., 1997. Ab initio potential functions for the ionic states of OH. *Chem. Phys. Letters* 276, 171–176.
- Oneal, D., Neff, J.E., 1997. OH 1.563 μm absorption from starspots on active stars. *Astron. J.* 113, 1129–1137.
- Pradhan, A. D. (1995) Private communication (to be published).
- Rodberg, L. S. and Thaler, R. M. (1967) *Introduction to the Quantum Theory of Scattering*. Academic Press, New York.
- Shizgal, B.D., Chen, H., 1996. The quadrature discretization method (QDM) in the solution of the Schrodinger equation with non-classical basis functions. *J. Chem. Phys.* 104, 4137–4150.
- Shizgal, B.D., 1997. The quadrature discretization method (QDM) in the calculation of the rotational–vibrational transitions in rare gas dimers. *Theochem.—J. Molec. Struc.* 391, 131.
- Shizgal, B.D., Arkos, G.G., 1996. Nonthermal escape of the atmospheres of Venus, Earth and Mars. *Rev. Geophys.* 34, 483–505.
- Szymczak, M., Lesqueren, A.M., 1995. A search for observational evidence of OH molecular photoproduction. *Mon. Not. R. Astron. Soc.* 276, 635.
- van Dishoeck, E.F., Langhoff, S.R., Dalgarno, A., 1983. The low-lying $^2\Sigma^-$ states of OH. *J. Chem. Phys.* 78, 4552–4561.
- van Dishoeck, E.F., Dalgarno, A., 1983. Photodissociation processes in the OH molecule. *J. Chem. Phys.* 79, 873–888.
- Vandop, H., Krol, M., 1996. Changing trends in tropospheric methane and carbon dioxide—a sensitivity analysis of the OH radical. *J. Atmos. Chem.* 25, 271.
- Wright, J.S., Donaldson, D.J., 1985. Potential energy and vibrational levels for local modes in water and acetylene. *Chem. Phys.* 94, 15–23.